Received: 28 April 2020 | Revised: 24 June 2020 | Accepted: 9 August 2020

DOI: 10.1002/que2.53

ORIGINAL PAPER

WILEY

Quantum simulation of clustered photosynthetic light harvesting in a superconducting quantum circuit

Ming-Jie Tao[1,2] | Ming Hua[3] | Na-Na Zhang[1] | Wan-Ting He[1] | Qing Ai[1] | Fu-Guo Deng[1,4]

[1]Department of Physics, Applied Optics Beijing Area Major Laboratory, Beijing Normal University, Beijing, China

[2]Faculty of Foundation, Space Engineering University, Beijing, China

[3]Department of Applied Physics, School of Physical Science and Technology, Tianjin Polytechnic University, Tianjin, China

[4]NAAM-Research Group, Department of Mathematics, Faculty of Science, King Abdulaziz University, Jeddah, Saudi Arabia

Correspondence
Qing Ai, Department of Physics, Applied Optics Beijing Area Major Laboratory, Beijing Normal University, Beijing 100875, China.
Email: aiqing@bnu.edu.cn

Funding information
National Natural Science Foundation of China, Grant/Award Number: 11674033, 11474026, 11505007, 11647042, and 11704281; Beijing Natural Science Foundation, Grant/Award Number: 1202017; China Postdoctoral Science Foundation, Grant/Award Number: 2018M631438

Summary

We propose a method to emulate the exciton energy transfer (EET) of photosynthetic complexes in a quantum superconducting circuit. Our system is composed of two pairs of superconducting charge qubits coupled to two separated high-Q superconducting transmission line resonators (TLRs), respectively. The two TLRs interact with each other capacitively. When the frequencies of the qubits are largely detuned from those of the TLRs, we simulate the process of EET from the first qubit to the fourth qubit. By tuning the couplings between the qubits and the TLRs, as well as the coupling between the two TLRs, we can modify the effective coupling strengths between the qubits and thus study the geometric effects on the EET. It is shown that a moderately clustered geometry supports optimal EET by using exciton delocalization and an energy matching condition. And the population loss during the EET has been trapped in the two TLRs.

KEYWORDS

exciton energy transfer, photosynthetic light harvesting, quantum simulation, superconducting quantum circuit

1 | INTRODUCTION

Energy plays an important role in modern society. The chemical energy supporting all lives on earth is mainly from the solar energy harvested by photosynthesis.[1-4] The solar energy can be captured and transferred to the reaction centers of photosynthetic systems in a short time with high efficiency.[1,5,6] Therefore, it might be beneficial to learn from the natural photosynthesis to design efficient artificial light-harvesting devices.

In the past few decades, many researches were focused on the study of the exciton energy transfer (EET) process in photosynthesis.[6-11] Based on the quantum dynamics of open systems,[2,12] much knowledge has been learned about the efficiency of the EET,[13-17] together with the spatial and energetic arrangement of the pigments.[18-22] The experimentally observed coherent phenomena in 2D spectroscopy may be attributed to nearly resonant coupling to an underdampped vibrational mode in the bath.[12,23] In natural photosynthesis, EET can be accomplished within 100 picoseconds with almost 100% efficiency.[24] Hu et al[25] observed that the bacteriochlorophylls involved in the overall excitation transfer

are found in a coplanar arrangement. Ishizaki and Fleming[26] showed that, by dimerization, the energy flow in the Fenna-Mattthew-Olson (FMO) complex occurs primarily through two EET pathways. Yang et al[27] found out that the dimerization in light-harvesting complex II (LH2) can effectively speed up the energy transfer between LH2 rings due to symmetry breaking. In a wheel-shaped artificial light-harvesting complex, the energy of the initially excited antenna can be efficiently directed to the reaction center, with quantum beating lasted for hundreds of femtoseconds.[28,29] In 2013, Ai et al[30] revealed that clustered geometry utilizes exciton delocalization and energy matching to optimize EET, which can be utilized to explain the efficient EET in FMO complex.[31]

In order to obtain the explicit relation between geometry and efficiency, some researches have explored random networks to discover some interesting findings.[32-34] Because the EET is sensitively influenced by the interference within the photosynthetic complex, even small changes in the geometry of the complex could turn constructive interference to destructive and thus result in significant drop in the efficiency. Pair sites renders EET properties robust against perturbations.[32] Compact structures tend to display high performance in the transport dynamics.[33] The networks characterized by Hamiltonians with centrosymmetry outperform those with completely random arrangements.[34] These discoveries seem to suggest that clustered geometries could favor efficient quantum transport.

On the other hand, much progress has been made in quantum information science, inspiring several interesting quantum simulation[35,36] experiments to verify the design principles for optimal light-harvesting.[28,29,37-42] By using bath engineering and the gradient ascent pulse engineering algorithm, Wang et al[37] performed an experimental quantum simulation of photosynthetic energy transfer by using nuclear magnetic resonance (NMR). It was demonstrated that the open quantum dynamics in an N-level system, with arbitrary Hamiltonian and bath spectral density, can be effectively emulated by an NMR system with $\log_2 N$ qubits.[38] Meanwhile, Gorman et al[43] showed in a trapped-ion system that the long-lived vibrational mode in the bath can assist the energy transfer. Superconducting quantum circuits provide another intriguing platform for quantum simulation.[44-51] In 2012, Mostame et al[39] simulated a complicated environment with a given spectral density for the EET in photosynthetic complexes by using inductor-resistor-capacitor oscillators. In 2018, Potočnik et al[40,41] experimentally demonstrated that light harvesting for a given geometry can be optimized by tuning the environmental noise.

However, although they have shown the potential of optimizing energy transfer by engineering the bath, none of them have experimentally demonstrated the effect of geometry on the EET efficiency. In Reference 30, it was shown that, in a linear geometry, moderate dimerization promotes the energy transfer. Therefore, it might be interesting to simulate the EET in different geometries to verify the design principals of optimal geometries. In this article, we design a system composed of four superconducting charge qubits and two superconducting transmission line resonators (TLRs). Here, two qubits form a pair and are coupled to one TLR. And the two TLRs are capacitively coupled with each other. Although there are no direct interactions between the qubits, the effective couplings among them can be induced by the simultaneous couplings to the common mode in each TLR.[52,53] Furthermore, the effective couplings can be tuned by adjusting the level spacings of the qubits, and their interaction strengths with the TLRs,[54] and the coupling strength between the two TLRs. In this way, we can investigate the EET for different geometries. Alternatively, for the sake of simplicity, the direct couplings between the qubits can be introduced instead. This alternative setup can simplify the arrangement and approximately simulate the EET dynamics for the parameter regime when the nearest-neighbor couplings dominate the transport.

This article is organized as follows: In the following section, we briefly introduce the theory for describing the EET in photosynthesis. In Section 3, we propose a setup consisting of four superconducting charge qubits and two TLRs to simulate the photosynthetic energy transfer. The effective Hamiltonian for the four qubits is obtained by the Fröhlich-Nakajima transformation. In Section 4, the energy transfer dynamics is numerically simulated by solving the Lindblad master equation, which confirms the previous investigation in Reference 30. Finally, the experimental feasibility and the main conclusions are discussed in Section 5.

2 | PHOTOSYNTHETIC LIGHT HARVESTING

In the photosynthesis with four chromophores, the EET is governed by the Frenkel-exciton Hamiltonian[1,30]

$$H = \sum_{j=1}^{4} \varepsilon_j |j\rangle\langle j| + \sum_{i\neq j=1}^{4} J_{ij} |i\rangle\langle j| + \text{h.c.}, \tag{1}$$

where ε_j is the site energy when jth chromophore is in the excited state, $|j\rangle$ is the state when jth chromophore is in the excited state while all other chromophores are in the ground state, J_{ij} is the dipole-dipole interaction between ith and jth chromophores.

Due to the strong coupling $J_{ij} \gtrsim |\varepsilon_i - \varepsilon_j|$, the exciton energy can coherently oscillate between any two sites i and j. However, because of the pure-dephasing-form system-bath Hamiltonian,

$$H_{SB} = \sum_{j,k} g_{jk} |j\rangle\langle j| (a_{jk}^{\dagger} + a_{jk}), \tag{2}$$

where g_{jk} is the coupling strength between jth chromophore and its local bath mode with frequency ω_k and creation (annihilation) operator $a_{jk}^{\dagger}$ (a_{jk}), the exciton energy can be irreversibly transferred to the target chromophore. In general, the system-bath coupling is described by the spectral density,

$$G(\omega) = \sum_{k} g_{jk}^2 \delta(\omega - \omega_k). \tag{3}$$

For a given geometry, the position $\vec{r}_j$ and transition dipole $\vec{\mu}_j$of every chromophore is fixed and thus the dipole-dipole interaction between any pair of two chromophores is determined by

$$J_{ij} = \frac{1}{4\pi\varepsilon_0 r_{ij}^3} [\vec{\mu}_i \cdot \vec{\mu}_j - 3(\vec{\mu}_i \cdot \hat{r}_{ij})(\vec{\mu}_j \cdot \hat{r}_{ij})], \tag{4}$$

where $\vec{r}_{ij} = r_{ij}\hat{r}_{ij} = \vec{r}_i - \vec{r}_j$ is the displacement vector from site j to site i, ε_0 is the vacuum permittivity. In addition, the spatial distribution of ε_j also facilitates the energy transfer by making use of the energy gradient towards the target chromophore, as shown in Figure 1B. In Reference 30, by using the coherent modified Redfield theory,[16,55,56] it is shown that, in a clustered geometry, exciton delocalization and energy matching cooperate to optimize EET.

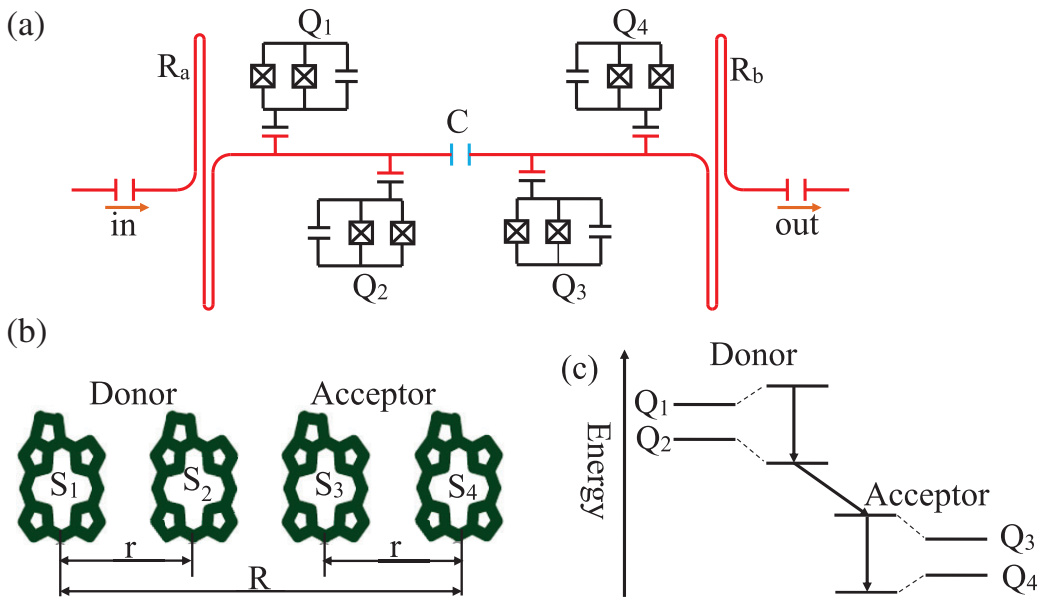

FIGURE 1 A, Schematic diagram of the superconducting circuit for simulating photosynthetic energy transfer. The two TLRs are capacitively coupled with each other. Charge qubits Q_1 and Q_2 form the donor, while qubits Q_3 and Q_4 act as the acceptor. Q_1 and Q_2 (Q_3 and Q_4) are capacitively coupled to TLR R_a (R_b). B, In a linear photosynthetic system, sites 1 and 2 form the donor pair, while sites 3 and 4 are the acceptor pair. The total distance between the two ends is fixed at R and the intrapair distance is r. C, Energy configuration of the four qubits for energy transfer, where only the excited states are involved in the EET and the ground states are not shown for simplicity. EET, exciton energy transfer; TLRs, transmission line resonators

3 | PHYSICAL SETUP

Let us consider a superconducting quantum circuit composed of four superconducting charge qubits and two 1D high-Q superconducting TLRs, as shown in Figure 1A. In order to study the cluster-to-cluster geometric effects, there should be two clusters at least, and two qubits can form a cluster. Therefore, four qubits are the minimum number of qubits to observe this effect. As shown in Figure 1B, we investigate the EET efficiency in a linear photosynthetic complex with four chromophores. The distance between the two ends is fixed at $R = 40\ \mathring{A}$, while sites 1 and 2 form the donor pair, and sites 3 and 4 are the acceptor pair, with intrapair distance $r < R/3$. The energy-level diagram of the four qubits is schematically shown in Figure 1C. Qubits Q_1 and Q_2 (Q_3 and Q_4) are coupled to the TLR R_a (R_b) capacitively. Here, we take Q_1 and Q_2 as donors because their energies are higher than those of the qubits Q_3 and Q_4, acting as acceptors. The effective couplings among these qubits exhibit the geometrical effects in photosynthetic complexes, because the couplings between pigments sensitively depend on their relative distances and orientations of electric dipoles. The couplings other than the nearest-neighbor couplings subtly modify the energy spectrum and thus the quantum dynamics. Furthermore, instead of direct couplings among qubits, we simplify the quantum circuit by introducing the additional TLRs. In other words, the TLRs play the role as the quantum data bus to induce the indirect couplings between the qubits. The frequencies of TLRs should be much smaller than the qubits to avoid the excitation of the TLRs. The distances between any two qubits are far enough to avoid direct interactions between them. Therefore, the energy is transferred from Q_1 to Q_4 by the indirect interactions among the qubits induced by simultaneously couplings to the common TLRs.

Under the rotating-wave approximation,[57] the Hamiltonian of the four qubits and two TLRs can be written as

$$\begin{aligned} H_1 = {} & \omega_a a^\dagger a + \sum_{j_1=1}^{2}\left[\frac{\omega_{j_1}}{2}\sigma_{j_1}^z + g_{j_1}(a^\dagger\sigma_{j_1}^- + a\sigma_{j_1}^+)\right] \\ & + \omega_b b^\dagger b + \sum_{j_2=3}^{4}\left[\frac{\omega_{j_2}}{2}\sigma_{j_2}^z + g_{j_2}(b^\dagger\sigma_{j_2}^- + b\sigma_{j_2}^+)\right] \\ & + g_a^b(a^\dagger + a)(b^\dagger + b), \end{aligned} \tag{5}$$

where ω_a, ω_b, ω_{j_1}, and ω_{j_2} are the transition frequencies of the TLRs R_a and R_b, and qubits Q_{j_s} ($s = 1, 2$), respectively. Here, $j_1 = 1, 2$ and $j_2 = 3, 4$. g_{j_1} (g_{j_2}) is the coupling strength between the qubit Q_{j_s} (Q_{j_2}) and the TLR R_a (R_b). g_a^b is the coupling strength between TLRs R_a and R_b. $a^\dagger$ and $b^\dagger$ are the creation operators of R_a and R_b, respectively. $\sigma_{j_s}^+ = |e\rangle_{j_s}\langle g|$ and $\sigma_{j_s}^z$ are the rising and Pauli operator of Q_{j_s}, respectively. $|g\rangle_{j_s}$ and $|e\rangle_{j_s}$ are the ground and excited states of Q_{j_s}, respectively.

By using the Fröhlich-Nakajima transformation[46]

$$U = \exp\left[\sum_{j_1=1}^{2}\frac{g_{j_1}}{\delta_{j_1}}(a^\dagger\sigma_{j_1}^- - a\sigma_{j_1}^+) + \sum_{j_2=3}^{4}\frac{g_{j_2}}{\delta_{j_2}}(b^\dagger\sigma_{j_2}^- - b\sigma_{j_2}^+)\right] \tag{6}$$

with $\delta_{j_1} = \omega_{j_1} - \omega_a \gg g_{j_1}$ and $\delta_{j_2} = \omega_{j_2} - \omega_b \gg g_{j_2}$, the original Hamiltonian of the system H_1 becomes

$$H_2 = U^\dagger H_1 U. \tag{7}$$

In the appendix, we give the detailed expression of H_2.

When the TLRs are initially prepared in the vacuum state and the high-order terms of g_{j_s}/δ_{j_s} can be omitted, the Hamiltonian H_2 can be reduced to

$$\begin{aligned} H_{eff} = {} & \sum_{j_1=1}^{2}\left(\omega_{j_1} + \frac{g_{j_1}^2}{\delta_{j_1}}\right)|e\rangle_{j_1}\langle e| + \sum_{j_2=3}^{4}\left(\omega_{j_2} + \frac{g_{j_2}^2}{\delta_{j_2}}\right)|e\rangle_{j_2}\langle e| \\ & + J_{12}(\sigma_1^-\sigma_2^+ + \sigma_1^+\sigma_2^-) + J_{34}(\sigma_3^-\sigma_4^+ + \sigma_3^+\sigma_4^-) \\ & + J_{23}(\sigma_2^-\sigma_3^+ + \sigma_2^+\sigma_3^-) + J_{13}(\sigma_1^-\sigma_3^+ + \sigma_1^+\sigma_3^-) \\ & + J_{24}(\sigma_2^-\sigma_4^+ + \sigma_2^+\sigma_4^-) + J_{14}(\sigma_1^-\sigma_4^+ + \sigma_1^+\sigma_4^-), \end{aligned} \tag{8}$$

where $J_{12} = \frac{g_1 g_2}{2\delta_1 \delta_2}(\delta_1 + \delta_2)$, $J_{34} = \frac{g_3 g_4}{2\delta_3 \delta_4}(\delta_3 + \delta_4)$, $J_{23} = \frac{g_a^b g_2 g_3}{\delta_2 \delta_3}$, $J_{13} = \frac{g_a^b g_1 g_3}{\delta_1 \delta_3}$, $J_{24} = \frac{g_a^b g_2 g_4}{\delta_2 \delta_4}$, and $J_{14} = \frac{g_a^b g_1 g_4}{\delta_1 \delta_4}$ are the indirect coupling strengths between any two qubits, respectively. In order to mimic the geometric effects, the effective couplings J_{ij}'s should be tunable. This can be achieved by adjusting detunings δ_j's, qubit-resonator couplings, and resonator-resonator coupling.[54]

When a quantum system interacts with a quantum bath, the states of the quantum system entangle with those of the quantum bath.[11] The correlation function of the classical bath is real-valued and time-symmetric. However, when a quantum system interacts with a quantum bath, the quantum system experiences time-dependent transition frequencies and thus results in a complex-valued time-asymmetric correlation function of the bath.[11] Due to this difference, the energy generally prefers to transfer from the higher-energy level to the lower-energy level of the quantum system interacting with a quantum bath.[11] Furthermore, the populations of all levels tend to be equal at the steady state in the case of a classical bath. The latter has been recently observed in the experimental NMR simulation.[37] In our configuration, the transition frequencies of the four qubits are assumed to satisfy the following relation, that is, $\left(\omega_1 + \frac{g_1^2}{\delta_1}\right) > \ldots > \left(\omega_4 + \frac{g_4^2}{\delta_4}\right)$, as shown in Figure 1B. Moreover, coupling strengths J_{12} and J_{34} are assumed to be larger than J_{23} to indicate that qubits Q_1 and Q_2 form the donor pair, while qubits Q_3 and Q_4 are the acceptor pair. For simplicity, we take $g_1 = g_4$, $g_2 = g_3$ and $\delta_1 \approx \delta_2 \approx \delta_3 \approx \delta_4$ to achieve $J_{12} = J_{34} > J_{23}$.[30] Thus, we use the following parameters $\omega_a/2\pi = \omega_b/2\pi = 3$ GHz, $\omega_1/2\pi = 13.115$ GHz, $\omega_2/2\pi = 13.009$ GHz, $\omega_3/2\pi = 12.991$ GHz, $\omega_4/2\pi = 13.078$ GHz[44,46] in our numerical simulations. The proposed parameters in the superconducting circuit model can be obtained from those found in biological systems by scaling down a factor 3×10^4.

4 | SIMULATION OF EET PROCESS

In the previous section, we obtain the effective Hamiltonian for the 4 qubits by the Fröhlich-Nakajima transformation and the rotating-wave approximation. It is reasonable to question the validity of rotating-wave approximation since there is strong coupling between the TLRs and the qubit-TLR couplings are relative large as compared with the frequencies of the TLRs. Hereafter, we shall numerically simulate quantum dynamics of the master equation under the exact Hamiltonian without the rotating-wave approximation.

In the interaction picture with respect to

$$H_0 = \omega_a a^\dagger a + \sum_{j_1=1}^{2} \frac{\omega_{j_1}}{2} \sigma_{j_1}^z + \omega_b b^\dagger b + \sum_{j_2=3}^{4} \frac{\omega_{j_2}}{2} \sigma_{j_2}^z, \tag{9}$$

we can derive the Lindblad-form master equation as References 16,58

$$\begin{aligned} \dot{\rho} = &-i[H_I, \rho] + \sum_{r=a,b} \kappa_r (N_r + 1) D[r]\rho + \sum_{r=a,b} \kappa_r N_r D[r^\dagger]\rho + \sum_{l=1}^{4} \Gamma_l^\gamma (N_l + 1) D[\sigma_l^-]\rho \\ &+ \sum_{l=1}^{4} \Gamma_l^\gamma N_l D[\sigma_l^+]\rho + \sum_{l=1}^{4} \Gamma_l^\phi D[\sigma_l^z]\rho, \end{aligned} \tag{10}$$

where the interaction Hamiltonian reads

$$H_I = \sum_{j=1}^{2} g_j (a\sigma_j^+ e^{i\delta_j t} + a^\dagger \sigma_j^+ e^{i(\omega_a + \omega_j)t}) + \sum_{j=3}^{4} g_j (b\sigma_j^+ e^{i\delta_j t} + b^\dagger \sigma_j^+ e^{i(\omega_b + \omega_j)t}) + g_a^b (abe^{-i\Delta_a^b t} + ab^\dagger e^{i\delta_a^b t}) + \text{h.c.}, \tag{11}$$

$$\delta_a^b = \omega_b - \omega_a, \tag{12}$$

$$\Delta_a^b = \omega_b + \omega_a, \tag{13}$$

$$D[A]\rho = (2A\rho A^\dagger - A^\dagger A\rho - \rho A^\dagger A)/2, \tag{14}$$

$$N_r = \frac{1}{\exp(\hbar\omega_r/k_BT) - 1}, \tag{15}$$

$$N_l = \frac{1}{\exp(\hbar\omega_l/k_BT)}, \tag{16}$$

κ_r $(r = a, b)$ is the leakage rate of TLR r, Γ_l^γ and Γ_l^ϕ $(l = 1, 2, 3, 4)$ are the spontaneous emission and pure-dephasing rates of the lth qubit, respectively.

In natural photosynthesis, the energy transfer is generally restricted in the single-excitation subspace. For simplicity, we label the bases as $|1\rangle = |e\rangle_1|g\rangle_2|g\rangle_3|g\rangle_4|0_a0_b\rangle$, $|2\rangle = |g\rangle_1|e\rangle_2|g\rangle_3g\rangle_4|0_a0_b\rangle$, $|3\rangle = |g\rangle_1|g\rangle_2|e\rangle_3|g\rangle_4|0_a0_b\rangle$, and $|4\rangle = |g\rangle_1|g\rangle_2|g\rangle_3|e\rangle_4|0_a0_b\rangle$. Here, $|n_an_b\rangle$ is the Fock state of TLR$_a$ and TLR$_b$. In addition, $|a\rangle = |g\rangle_1|g\rangle_2|g\rangle_3|g\rangle_4|1_a0_b\rangle$ and $|b\rangle = |g\rangle_1|g\rangle_2|g\rangle_3|g\rangle_4|0_a1_b\rangle$ indicate single-excitation in one of the TLRs. In our simulation, the system composed of four superconducting qubits and two TLRs is initially prepared at the state $|1\rangle$. In Figure 2, we show the time evolution of the populations of single-excitation states of the four qubits $P_m = \langle m|\rho|m\rangle$ $(m = 1, 2, 3, 4)$. In a realistic experiment, each qubit can be dispersively coupled to a TLR. The qubit's population can be extracted by measuring the phase of the signal in the TLR.[59] And the qubit's decay time will not be significantly modified by Purcell-like couplings to the TLRs, which will be discussed in detail in Section 5. Here, we take $1/\Gamma_j^\gamma = 3$ μs and $1/\Gamma_j^\phi = 70$ ns $(j = 1, 2, 3, 4)$,[59] which meet the requirement $\Gamma_j^\phi \gg \Gamma_j^\gamma$.[60-62] The leakage rates of two TLRs are $\kappa_a^{-1} = \kappa_b^{-1} = 10$ μs.[63]

In Figure 2, we demonstrate the population dynamics of the four qubits for three different geometries, corresponding to three different sets of nearest-neighbor couplings J_{12}, J_{34}, and J_{23}. In Reference 30, it has been proven that the next-nearest-neighbor couplings J_{13} and J_{24}, and the end-to-end coupling J_{14} plays a minor role in the EET. First of all, we would like to simulate the energy transfer for an equal-coupling geometry. Therefore, we investigate the energy transfer dynamics of the system with approximately equal-coupling strengths between adjacent qubits in Figure 2A. It

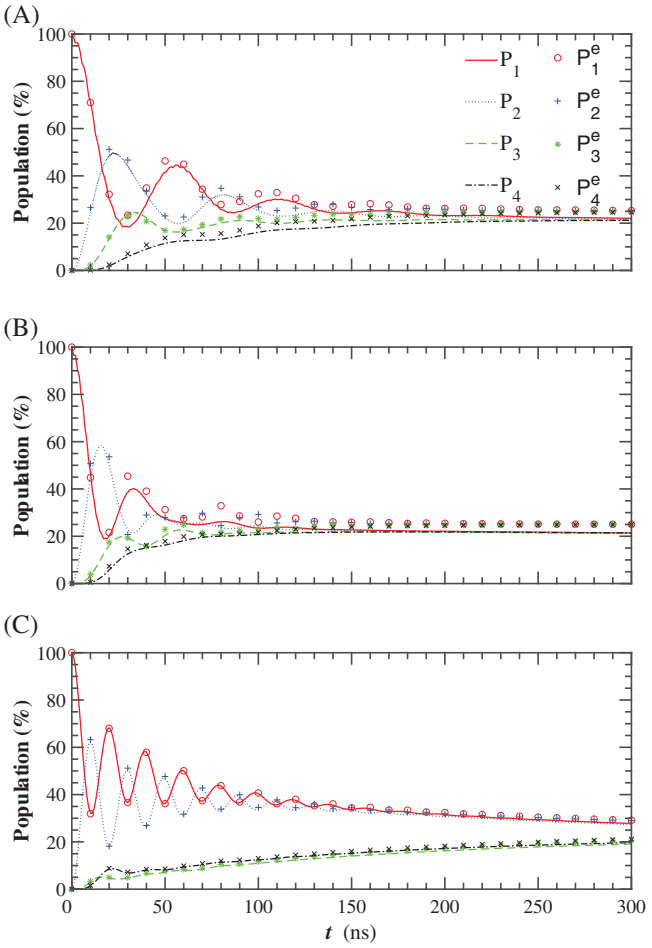

FIGURE 2 The curves (symbol) show the propagation of the populations of excitation on each of the four qubits by $H_{\rm I}$ ($H_{\rm eff}$) for three different geometries: A, equally spaced geometry with $J_{12} = J_{34} \approx J_{23}$ and $r \approx R/3$, B, moderately clustered geometry with $J_{12} = J_{34} = 1.62J_{23}$ and $r < R/3$, C, overclustered geometry with $J_{12} = J_{34} = 3.11J_{23}$ and $r \ll R/3$. The red solid line (∘) is for P_1 ($P_1^{\rm e}$), blue dotted line (+) for P_2 ($P_2^{\rm e}$), green dashed line (*) for P_3 ($P_3^{\rm e}$), and black dash-dotted line (×) for P_4 ($P_4^{\rm e}$)

corresponds to the equally spaced geometry in Reference 30. In order to achieve $J_{12} = J_{34} \approx J_{23}$, coupling strengths are assumed to be $g_1/2\pi = g_4/2\pi = 100$ MHz, $g_2/2\pi = g_3/2\pi = 990$ MHz, and $g_b^a/2\pi = 980$ MHz. In this case, the energy transfer can be accomplished within about 300 ns. Figure 2B simulates the energy transfer dynamics in the moderately clustered geometry with $J_{12} = J_{34} = 1.62J_{23}$. Here, we adopt $g_1/2\pi = g_4/2\pi = 150$ MHz, $g_2/2\pi = g_3/2\pi = 990$ MHz, and $g_b^a = 930$ MHz. Compared with Figure 2A, the energy transfer from the first qubit to the last one can be completed within a shorter time, that is, approximately 150 ns. The moderately clustered geometry supports a faster energy transfer because the enhanced couplings within the cluster enlarge the intracluster energy gap and reduce the intercluster energy gap. Both the strong coherent hopping within the cluster and the resonant energy transfer between the two clusters accelerate the overall energy transfer. Moreover, when the ratio J_{12}/J_{23} increases to a larger value, for example, $J_{12} = J_{34} = 3.11J_{23}$ for $g_1/2\pi = g_4/2\pi = 230$ MHz, $g_2/2\pi = g_3/2\pi = 920$ MHz, and $g_b^a = 800$ MHz, the energy transfer becomes extremely slow and it does not finish even at 300 ns, as shown in Figure 2C. That's because the strong intracluster couplings enlarge the intracluster energy gap excessively and thus increase the intercluster energy gap. In order to find out the optimal parameters for the EET efficiency, we simulate the EET dynamics of our circuit for a broad range of the parameters g_1, g_2, and g_b^a with $g_1 = g_4$ and $g_2 = g_3$ and keeping other parameters unchanged. The parameters are changed from 10 MHz to 990 MHz with 10 MHz step. According to the numerical simulations, we find that the optimal energy transfer occurs at $J_{12} = J_{34} = 1.62J_{23}$, as shown in Figure 2B.

In Figure 2, there are coherent oscillations in the short-time regime, which correspond to the quantum coherence phenomena discovered in 2D spectroscopy experiments.[1,64] Because there is strong coupling between the two donor (acceptor) qubits, the energy gap between their eigen-states will be opened up, that is, $|\varepsilon_1\rangle$ and $|\varepsilon_2\rangle$, as shown in Figure 1B. And the energy coherently moves within the donor cluster. However, since the couplings between the donor and acceptor clusters are relatively weak, the energy will incoherently hop between the clusters. According to Förster theory,[65,66] the energy transfer rate from the lower donors' eigen-state $|\varepsilon_2\rangle$ to the higher acceptors' eigen-state $|\varepsilon_3\rangle$ is integral of donor's emission spectrum and acceptor's absorption spectrum. The former is centered at the lower donors' eigen-state, and the latter is centered at the higher acceptors' eigen-state. When the coupling within the donor (acceptor) pair is moderately enlarged, cf. Figure 3A vs B, the energy gap between $|\varepsilon_2\rangle$ and $|\varepsilon_3\rangle$ has been reduced, and thus results in an enhanced transfer rate. In this way, the clustered geometries utilize energy matching to optimize energy transfer between two clusters. However, if the coupling within the donor (acceptor) pair is overenlarged, cf. Figure 3C, this may suppress the transfer rate as the energies of two states mismatch.[11] Moreover, strong coupling between a charge qubit and a TLR can be achieved in superconducting circuit.[67-69]

In Figure 2, we also show the quantum simulations by H_{eff}. The simulations by H_{eff} coincide with those by H_{I} in the aspects of oscillation frequency and energy transfer rate. We notice that in Figure 2B, the population of each qubit is about 24%, when the circuit is in the steady-state. To explore the reason why the summation of all the populations of the four qubits cannot reach 100%, we plot the time evolution of populations in the TLRs $P_a = \langle 1_a|\rho|1_a\rangle$and $P_b = \langle 1_b|\rho|1_b\rangle$ in Figure 4. It is shown that after some oscillations in the short-time regime, P_a and P_b increase linearly in time. And both of them reach about 2% at 150 ns. Therefore, since only a small portion of the population, which has not been transferred to the target qubit, has been trapped in the two TLRs, our simulation approach can effectively mimic the EET in the 4-chromophore linear photosynthetic complex, as shown in Figure 1B.

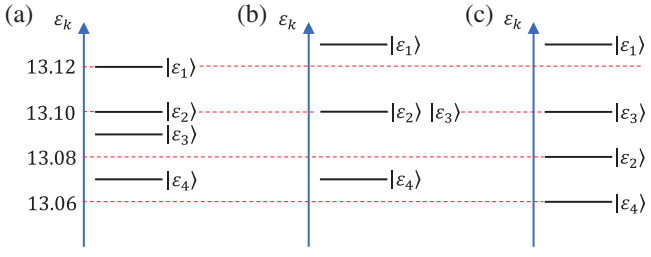

FIGURE 3 The energy-level diagrams corresponding to quantum dynamics in Figure 2: A, Equally spaced geometry with $J_{12} = J_{34} \approx J_{23}$ and $r \approx R/3$, B, moderately clustered geometry with $J_{12} = J_{34} = 1.62J_{23}$ and $r < R/3$, C, overclustered geometry with $J_{12} = J_{34} = 3.11J_{23}$ and $r \ll R/3$. r and R are respectively, the intrapair distance and the distance between the two ends in Figure 1B.

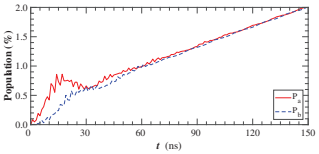

FIGURE 4 The populations trapped in the TLRs P_a (P_b) vs time. TLRs, transmission line resonators

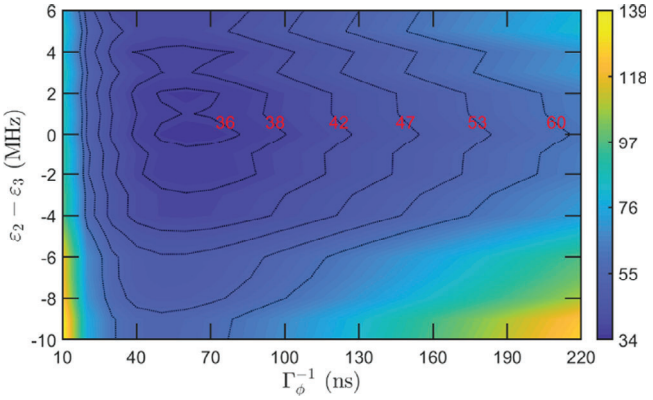

FIGURE 5 The transfer time τ vs the detuning $\Delta = \varepsilon_2 - \varepsilon_3$ between the lower eigen-state $|\varepsilon_2\rangle$ of $|1\rangle$ and $|2\rangle$, and the higher eigen-state $|\varepsilon_3\rangle$ of $|3\rangle$ and $|4\rangle$, and the dephasing time Γ_ϕ^{-1}

Figures 2 and 3 clearly show the dependence of transfer time τ on the detuning $\Delta = \varepsilon_2 - \varepsilon_3$ between the lower eigen-state $|\varepsilon_2\rangle$ of $|1\rangle$ and $|2\rangle$, and the higher eigen-state $|\varepsilon_3\rangle$ of $|3\rangle$ and $|4\rangle$. And the previous discoveries[39,43] suggested the design of bath can also optimize the energy transfer. Therefore, we investigate the energy transfer for a broad range of Δ and the dephasing time Γ_ϕ^{-1}, as shown in Figure 5. By using a two-exponential-decay model in Reference 30,

$$P_4(t) = a_L(1 - e^{-t/\tau}) + a_S(1 - e^{-t/\tau'}), \tag{17}$$

where $a_L \gg a_S$, we numerically fit the population dynamics of qubit 4, and effectively obtain the transfer time τ. We may identify the optimal transfer time $\tau_{\text{opt}} = 35.03$ ns at $\Delta = 0$ and $\Gamma_\phi^{-1} = 60$ ns. First of all, we explore the relation between τ and Δ, for a fixed Γ_ϕ^{-1}. When Δ is decreased from a large positive detuning, the transfer time experiences a decrease as $|\varepsilon_2\rangle$ and $|\varepsilon_3\rangle$ approach the energy matching, that is, $\Delta = 0$. However, if Δ further decreases, the transfer time increases since the two states become more and more mismatched. On the other hand, we also explore the relation between τ and Γ_ϕ^{-1}, for a fixed Δ, that is, in a given geometry. By tuning Γ_ϕ^{-1}, the system gradually reaches optimal transfer time at $\Gamma_\phi \simeq 16.7$ MHz, which is comparable to the effective coupling $J_{23} = 8.87$ MHz between $|2\rangle$ and $|3\rangle$. In the coherent-dynamics limit, that is, $\Gamma_\phi^{-1} \to \infty$, because the population will oscillate backwards and forwards, the energy cannot be effectively transferred. In the opposite case, when $\Gamma_\phi^{-1} \to 0$, since the strong system-bath couplings frequently probe the qubits' populations, the dynamic localization freezes the population dynamics.[60-62] In other words, the quantum Zeno effect[70,71] prohibits the effective energy transfer.

5 | DISCUSSION AND SUMMARY

In this article, instead of direct couplings among two neighboring qubits, we explore two additional TLRs to induce the couplings among any two qubits. In linear geometries, there are next-nearest-neighbor couplings besides the nearest-neighbor couplings. This architecture also enables us to simulate photosynthetic complexes beyond the linear geometries in Reference 30, since natural photosynthetic complexes possess more interesting geometries, such as ring-shape LH1(LH2), FMO, and photosystem I(II). Furthermore, by using TLRs, we can simplify the quantum circuit for nonlinear geometries beyond the nearest-neighbor couplings.

In our simulations, we select the charge qubits with the dissipation time $T_1 = 200$ μs,[59] which is much longer than their pure-dephasing time $T_2 = 0.07$ μs,[59] because in dephasing-assisted photosynthetic energy transport the spontaneous fluorescence can be ignored.[60-62] However, since the energy transfer generally completes within 0.3 μs, for example, in Figure 2A,B, a much shorter dissipation time, for example, $T_1 = 3$ μs, is enough to obtain the same simulations in realistic experiments. This has been confirmed by our numerical simulations which are not shown here. Furthermore, due to couplings to the TLRs, the qubits' decay times may be shortened due to Purcell effect. In Reference 72, the Purcell decay rate is analytically estimated as

$$\Gamma = \frac{\kappa}{2} - \frac{\sqrt{2}}{2}\sqrt{-A + \sqrt{A^2 + (\kappa\Delta)^2}}, \tag{18}$$

where

$$A^2 = \Delta^2 + 4g^2 - \kappa^2/4, \tag{19}$$

κ^{-1} is the decay time of the TLR, Δ is the detuning between the qubit and TLR, g is the coupling strength. Because the qubits dispersively couple with the TLRs, that is, $g/\Delta \ll 1$, $\Gamma \simeq \kappa g^2/\Delta^2$ to the lowest order of g/Δ. For the present parameters, the Purcell decay time is about 2 ms, which is much longer than 4 μs. Therefore, the Purcell effect will not significantly modify the qubits' decay times.

Parameters used here have been realized in experiments. The quality factor of a superconducting TLR can reach 10^5.[73] The frequency of the fundamental mode of the TLR can be designed from 1 to 10 GHz.[46,74,75] The frequency of a superconducting charge qubit can be effectively tuned from 5 to 15 GHz, by varying the flux that applied though the loop of the qubit.[46] In addition, the ultra-strong coupling between a charge qubit and a TLR is achieved when $\min\{g_j\} \gg \sqrt{\kappa_\alpha \Gamma_j^\gamma}$ $(j = 1, 2, 3, 4, \alpha = a, b)$.[76] Although the coupling strength reaches the ultra-strong regime, that is, $g_j/\omega_a \simeq 1/3$, the Jaynes-Cumming model is still valid as the large-detuning condition still holds.[77] As a result, the population dynamics will not be essentially modified.

In Reference 37, the NMR experimental simulation was compared with the numerically exact simulation using the hierarchical equation of motion (HEOM).[26,78] Here, in our configuration, there are two TLRs in addition to 4 qubits. The presence of extra modes in the TLRs results in the increasing complexity of the quantum master equation, which can be solved by using QuTiP,[79,80] as compared with the HEOM for four chlorophylls.

In natural photosynthetic complexes, the energy is transferred from the outer antenna to the reaction center across tens of nanometers.[1,30,37] There is a large energy gap between the lowest eigen-state of the outer antenna and the reaction center, which can prevent the back transfer of energy. As a result, the transfer rate from the lowest-energy state to the reaction center is much smaller than the transfer rate within the outer antenna.[37,81] In this work, it is thus reasonable to simulate the energy transfer without the reaction center. However, a TLR can be utilized to effectively simulate the reaction center. Coupled to some specific qubit, the TLR can act as a reaction center through Purcell-like coupling.[40,41] By tuning the TLR's decay time and the qubit-TLR detuning, we can effectively modified the qubit's decay time through Purcell-like coupling, according to Equation (18).

In summary, we have proposed a simulation scheme for demonstrating geometric effects on the photosynthetic EET in four superconducting charge qubits plus two separated high-Q TLRs. The loss of population during the EET is trapped in the TLRs. In the future work, it might be interesting to demonstrate the effect of fluorescence on the EET by varying the couplings between the qubits and the TLRs.

ACKNOWLEDGEMENTS

This work was supported by National Natural Science Foundation of China under Grant Nos. 11674033, 11474026, 11505007, and Beijing Natural Science Foundation under Grant No. 1202017. M.H. was supported by the National Natural Science Foundation of China under Grant Nos. 11647042 and 11704281. M.J.T. was supported by the China Postdoctoral Science Foundation under Grant No. 2018M631438.

REFERENCES

1. Cheng YC, Fleming GR. Dynamics of light harvesting in photosynthesis. *Annu Rev Phys Chem*. 2009;60:241-262.
2. Lambert N, Chen YN, Cheng YC, Li CM, Chen GY, Nori F. Quantum biology. *Nat Phys*. 2013;9:10-18.
3. Chin AW, Prior J, Rosenbach R, Caycedo-Soler F, Huelga SF, Plenio MB. The role of non-equilibrium vibrational structures in electronic coherence and recoherence in pigment-protein complexes. *Nat Phys*. 2013;9:113-118.
4. Blankenship RE. *Molecular Mechanisms of Photosynthesis*. Oxford, UK: Wiley-Blackwell; 2002.
5. Cheng YC, Silbey RJ. Coherence in the B800 ring of purple bacteria LH2. *Phys Rev Lett*. 2006;96:028103.
6. Engel GS, Calhoun TR, Read EL, et al. Evidence for wavelike energy transfer through quantum coherence in photosynthetic systems. *Nature*. 2007;446:782-786.
7. van Amerongen H, Valkunas L, van Grondelle R. *Photosynthetic Excitons*. Singapore: World Scientific; 2000.
8. Knox RS. Electronic excitation transfer in the photosynthetic unit. *Photosynth Res*. 1996;48:35-39.
9. Leegwater JA. Coherent versus incoherent energy transfer and trapping in photosynthetic antenna complexes. *J Phys Chem*. 1996;100:14403-14409.
10. Savikhin S, Buck DR, Struve WS. Oscillating anisotropies in a bacteriochlorophyll protein. *Chem Phys*. 1997;223:303-312.
11. Mančal T. Excitation energy transfer in a classical analogue of photosynthetic antennae. *J Phys Chem B*. 2013;117:11282-11291.
12. Cao J, Cogdell RJ, Coker DF, et al. Quantum biology revisited. *Sci Adv*. 2020;6:eaaz4888.

13. Jang S, Hoyer S, Fleming GR, Whaley KB. Non-Markovian multichromophoric förster resonance energy transfer for modular exciton densities. *Phys Rev Lett*. 2014;113:188102.
14. Fassioli F, Olaya-Castro A, Scholes GD. Coherent energy transfer under incoherent light conditions. *J Phys Chem Lett*. 2012;3:3136-3142.
15. Collini E, Wong CY, Wilk KE, Curmi PMG, Brumer P, Scholes GD. Coherently wired light-harvesting in photosynthetic marine algae at ambient temperature. *Nature*. 2010;463:644-647.
16. Ai Q, Fan YJ, Jin BY, Cheng YC. An efficient quantum jump method for coherent energy transfer dynamics in photosynthetic systems under the influence of laser fields. *New J Phys*. 2014;16:053033.
17. Hildner R, Brinks D, Nieder JB, Cogdell RJ, van Hulst NF. Quantum coherent energy transfer over varying pathways in single light-harvesting complexes. *Science*. 2013;340:1448-1451.
18. Sener MK, Struempfer J, Hsin J, et al. Förster energy transfer theory as reflected in the structures of photosynthetic light-harvesting systems. *ChemPhysChem*. 2011;12:518-531.
19. Scholak T, de Melo F, Wellens T, Mintert F, Buchleitner A. Efficient and coherent excitation transfer across disordered molecular networks. *Phys Rev E*. 2011;83:021912.
20. Marin A, Doust AB, Scholes GD, et al. Flow of excitation energy in the cryptophyte light-harvesting antenna phycocyanin 645. *Biophys J*. 2011;101:1004-1113.
21. Cleary L, Chen H, Chuang C, Silbey RJ, Cao J. Optimal fold symmetry of LH2 on a photosynthetic membrane. *Proc Natl Acad Sci U S A*. 2013;110:8537-8542.
22. Xu L, Gong ZR, Tao MJ, Ai Q. Artificial light harvesting by dimerized möbius ring. *Phys Rev E*. 2018;97:042124.
23. Mourokh LG, Nori F. Energy transfer efficiency in the chromophore network strongly coupled to a vibrational mode. *Phys Rev E*. 2015;92:052720.
24. Fleming GR, van Grondelle R. The primary steps of photosynthesis. *Phys Today*. 1994;47(2):48-55.
25. Hu X, Ritz T, Damjanovic A, Schulten K. Pigment organization and transfer of electronic excitation in the photosynthetic unit of purple bacteria. *J Phys Chem B*. 1997;101:3854-3871.
26. Ishizaki A, Fleming GR. Theoretical examination of quantum coherence in a photosynthetic system at physiological temperature. *Proc Natl Acad Sci U S A*. 2009;106:17255-17260.
27. Yang S, Xu DZ, Song Z, Sun CP. Dimerization-assisted energy transport in light-harvesting complexes. *J Chem Phys*. 2010;132:234501.
28. Ghosh PK, Smirnov AY, Nori F. Quantum effects in energy and charge transfer in an artificial photosynthetic complex. *J Chem Phys*. 2011;134:244103.
29. Ghosh PK, Smirnov AY, Nori F. Artificial photosynthetic reaction centers coupled to light-harvesting antennas. *Phys Rev E*. 2011;84:061138.
30. Ai Q, Yen TC, Jin BY, Cheng YC. Clustered geometries exploiting quantum coherence effects for efficient energy transfer in light harvesting. *J Chem Phys Lett*. 2013;4:2577-2584.
31. Chen GY, Lambert N, Li CM, Chen YN, Nori F. Rerouting excitation transfers in the Fenna-Matthews-Olson complex. *Phys Rev E*. 2013;88:032120.
32. Mostarda S, Levi F, Prada-Gracia D, Mintert F, Rao F. Structure-dynamics relationship in coherent transport through disordered systems. *Nat Commun*. 2013;4:2296.
33. Knee GC, Rowe P, Smith LD, Troisi A, Datta A. Structure-dynamics relation in physically-plausible multi-chromophore systems. *J Phys Chem Lett*. 2017;8:2328-2333.
34. Zech T, Mulet R, Wellens T, Buchleitner A. Centrosymmetry enhances quantum transport in disordered molecular networks. *New J Phys*. 2014;16:055002.
35. Buluta I, Nori F. Quantum simulators. *Science*. 2009;326:108-111.
36. Georgescu I, Ashhab S, Nori F. Quantum simulation. *Rev Mod Phys*. 2014;86:153-185.
37. Wang BX, Tao MJ, Ai Q, et al. Efficient quantum simulation of photosynthetic light harvesting. *NPJ Quantum Inf*. 2018;4:52.
38. Zhang NN, Tao MJ, He WT, Chen XY, Kong XY, Deng FG, Lambert N, Ai Q, Cheng YC. Exact and efficient quantum simulation of open quantum dynamics for various of hamiltonians and spectral densities; 2020. arXiv:2007.02303.
39. Mostame S, Rebentrost P, Eisfeld A, Kerman AJ, Tsomokos DI, Aspuru-Guzik A. Quantum simulator of an open quantum system using superconducting qubits: exciton transport in photosynthetic complexes. *New J Phys*. 2012;14:105013.
40. Potočnik A, Bargerbos A, Schröder FAYN, et al. Studying light-harvesting models with superconducting circuits. *Nat Commun*. 2018;9:904.
41. Chin AW, Mangaud E, Atabek O, Desouter-Lecomte M. Coherent quantum dynamics launched by incoherent relaxation in a quantum circuit simulator of a light-harvesting complex. *Phys Rev A*. 2018;97:063823.
42. del Rey M, Chin AW, Huelga SF, Plenio MB. Exploiting structured environments for efficient energy transfer: the phonon antenna mechanism. *J Phys Chem Lett*. 2013;4:903-907.
43. Gorman DJ, Hemmerling B, Megidish E, et al. Engineering vibrationally assisted energy transfer in a trapped-ion quantum simulator. *Phys Rev X*. 2018;8:011038.
44. Blais A, Huang RS, Wallraff A, Girvin SM, Schoelkopf RJ. Cavity quantum electrodynamics for superconducting electrical circuits: an architecture for quantum computation. *Phys Rev A*. 2004;69:062320.
45. You JQ, Nori F. Superconducting circuits and quantum information. *Phys Today*. 2005;58(11):42-47.
46. Blais A, Gambetta J, Wallraff A, et al. Quantum-information processing with circuit quantum electrodynamics. *Phys Rev A*. 2007;75:032329.
47. Leek PJ, Fink JM, Blais A, et al. Observation of Berry's phase in a solid-state qubit. *Science*. 2007;318:1889-1892.
48. Ai Q, Huo WY, Long GL, Sun CP. Nonadiabatic fluctuation in the measured geometric phase. *Phys Rev A*. 2009;80:024101.
49. You JQ, Nori F. Atomic physics and quantum optics using superconducting circuits. *Nature*. 2011;474:589-597.

50. Xiang ZL, Ashhab S, You JQ, Nori F. Hybrid quantum circuits: superconducting circuits interacting with other quantum systems. *Rev Mod Phys*. 2013;85:623-653.
51. Gu X, Kockum AF, Miranowicz A, Liu YX, Nori F. Microwave photonics with superconducting quantum circuits. *Phys Rep*. 2017;718:1-102.
52. Yang CP, Su QP, Nori F. Entanglement generation and quantum information transfer between spatially-separated qubits in different cavities. *New J Phys*. 2013;15:115003.
53. Yang CP, Su QP, Zheng SB, Nori F. Entangling superconducting qubits in a multi-cavity system. *New J Phys*. 2016;18:013025.
54. Allman MS, Altomare F, Whittaker JD, et al. Simmonds RW rf-SQUID-mediated coherent tunable coupling between a superconducting phase qubit and a lumped-element resonator. *Phys Rev Lett*. 2010;104:177004.
55. Hwang-Fu YH, Chen W, Cheng YC. A coherent modified redfield theory for excitation energy transfer in molecular aggregates. *Chem Phys*. 2015;447:46-53.
56. Chang Y, Cheng YC. On the accuracy of coherent modified redfield theory in simulating excitation energy transfer dynamics. *J Chem Phys*. 2015;142:034109.
57. Ai Q, Li Y, Zheng H, Sun CP. Quantum anti-zeno effect without rotating wave approximation. *Phys Rev A*. 2010;81:042116.
58. Breuer HP, Petruccione F. *The Theory of Open Quantum Systems*. New York, NY: Oxford University Press; 2002.
59. Kim Z, Suri B, Zaretskey V, et al. Decoupling a cooper-pair box to enhance the lifetime to 0.2 ms. *Phys Rev Lett*. 2011;106:120501.
60. Plenio MB, Huelga SF. Dephasing-assisted transport: quantum networks and biomolecules. *New J Phys*. 2008;10:113019.
61. Rebentrost P, Mohseni M, Kassal I, Lloyd S, Aspuru-Guzik A. Environment-assisted quantum transport. *New J Phys*. 2009;11:033003.
62. Chin AW, Datta A, Caruso F, Huelga SF, Plenio MB. Noise-assisted energy transfer in quantum networks and light-harvesting complexes. *New J Phys*. 2010;12:065002.
63. Wallraff A, Schuster DI, Blais A, et al. Approaching unit visibility for control of a superconducting qubit with dispersive readout. *Phys Rev Lett*. 2005;95:060501.
64. Pachon LA, Brumer P. Computational methodologies and physical insights into electronic energy transfer in photosynthetic light-harvesting complexes. *Phys Chem Chem Phys*. 2012;14:10094-10108.
65. Valkunas L, Abramavicius D, Mančal T. *Molecular Excitation Dynamics and Relaxation: Quantum Theory and Spectroscopy*. Weinheim: Wiley-VCH; 2013.
66. May V, Kühn O. *Charge and Energy Transfer Dynamics in Molecular Systems*. 3rd ed. Weinheim: Wiley-VCH; 2011.
67. Ashhab S, Nori F. Qubit-oscillator systems in the ultrastrong-coupling regime and their potential for preparing nonclassical states. *Phys Rev A*. 2010;81:042311.
68. Fay A, Hoskinson E, Lecocq F, et al. Strong tunable coupling between a superconducting charge and phase qubit. *Phys Rev Lett*. 2008;100:187003.
69. Nataf P, Ciuti C. Vacuum degeneracy of a circuit QED system in the ultrastrong coupling regime. *Phys Rev Lett*. 2010;104:023601.
70. Kofman AG, Ashhab S, Nori F. Nonperturbative theory of weak pre- and post-selected measurements. *Phys Rep*. 2012;520:43-133.
71. Ai Q, Xu DZ, Yi S, Kofman AG, Sun CP, Nori F. Quantum anti-zeno effect without wave function reduction. *Sci Rep*. 2013;3:1752.
72. Sete EA, Gambetta JM, Korotkov AN. Purcell effect with microwave drive: suppression of qubit relaxation rate. *Phys Rev B*. 2014;89:104516.
73. Megrant A, Neill C, Barends R, et al. Planar superconducting resonators with internal quality factors above one million. *Appl Phys Lett*. 2012;100:113510.
74. LaHaye MD, Buu O, Camarota B, Schwab KC. Approaching the quantum limit of a nanomechanical resonator. *Science*. 2004;304:74-77.
75. Gaidarzhy A, Zolfagharkhani G, Badzey RL, Mohanty P. Evidence for quantized displacement in macroscopic nanomechanical oscillators. *Phys Rev Lett*. 2005;94:030402.
76. Haroche S. *Fundamental Systems in Quantum Optics*. Berlin, Germany: Spinger-Verlag; 1994.
77. Kockum A, Miranowicz A, Liberato S, Savasta S, Nori F. Ultrastrong coupling between light and matter. *Nat Rev Phys*. 2019;1:19-40.
78. Tao MJ, Zhang NN, Wen PY, Deng FG, Ai Q, Long GL. Coherent and incoherent theories for photosynthetic energy transfer. *Sci Bull*. 2020;65:318-328.
79. Johansson JR, Nation PD, Nori F. QuTiP2: an open-source python framework for the dynamics of open quantum systems. *Comput Phys Commun*. 2013;184:1234-1240.
80. Johansson JR, Nation PD, Nori F. QuTiP: an open-source python framework for the dynamics of open quantum systems. *Comput Phys Commun*. 2012;183:1760-1772.
81. Moix JM, Zhao Y, Cao JS. Equilibrium-reduced density matrix formulation: influence of noise, disorder, and temperature on localization in excitonic systems. *Phys Rev B*. 2012;85:115412.

How to cite this article: Tao M-J, Hua M, Zhang N-N, He W-T, Ai Q, Deng F-G. Quantum simulation of clustered photosynthetic light harvesting in a superconducting quantum circuit. *Quantum Engineering*. 2020;e53. https://doi.org/10.1002/que2.53

APPENDIX A. COMPLETE EXPRESSION OF H_2

Here, we give the detailed expression of H_2 used in Section 3. We can omit the high-order terms of g_{j_s}/δ_{j_s} and simplify

$$H_2 = U^{\dagger} H_1 U \tag{A1}$$

as

$$\begin{aligned}
H_2 = {} & \omega_a a^{\dagger} a + \omega_b b^{\dagger} b + g_a^b (a^{\dagger} + a)(b^{\dagger} + b) \\
& + \sum_{j_1=1}^{2} \frac{g_a^b g_{j_1}^2}{2\delta_{j_1}^2} (a^{\dagger} + a)(b^{\dagger} + b)\sigma_{j_1}^z \\
& + \sum_{j_2=3}^{4} \frac{g_a^b g_{j_2}^2}{2\delta_{j_2}^2} (a^{\dagger} + a)(b^{\dagger} + b)\sigma_{j_2}^z \\
& + \sum_{j_1=1}^{2} \left[\frac{\omega_{j_1}}{2}\sigma_{j_1}^z + \frac{g_{j_1}^2}{\delta_{j_1}} (a a^{\dagger} \sigma_{j_1}^+ \sigma_{j_1}^- - a^{\dagger} a \sigma_{j_1}^- \sigma_{j_1}^+) \right. \\
& \left. + \frac{g_a^b g_{j_1}}{\delta_{j_1}} (b^{\dagger} \sigma_{j_1}^- + b \sigma_{j_1}^+) \right] + \frac{g_1 g_2}{2\delta_1 \delta_2} (\delta_1 + \delta_2)(\sigma_1^- \sigma_2^+ + \sigma_1^+ \sigma_2^-) \\
& + \sum_{j_2=3}^{4} \left[\frac{\omega_{j_2}}{2}\sigma_{j_2}^z + \frac{g_{j_2}^2}{\delta_{j_2}} (b b^{\dagger} \sigma_{j_2}^+ \sigma_{j_2}^- - b^{\dagger} b \sigma_{j_2}^- \sigma_{j_2}^+) \right. \\
& \left. + \frac{g_a^b g_{j_2}}{\delta_{j_2}} (a^{\dagger} \sigma_{j_2}^- + a \sigma_{j_2}^+) \right] + \frac{g_3 g_4}{2\delta_3 \delta_4} (\delta_3 + \delta_4)(\sigma_3^- \sigma_4^+ + \sigma_3^+ \sigma_4^-) \\
& + \frac{g_a^b g_1 g_3}{\delta_1 \delta_3} (\sigma_1^- \sigma_3^+ + \sigma_1^+ \sigma_3^-) + \frac{g_a^b g_1 g_4}{\delta_1 \delta_4} (\sigma_1^- \sigma_4^+ + \sigma_1^+ \sigma_4^-) \\
& + \frac{g_a^b g_2 g_3}{\delta_2 \delta_3} (\sigma_2^- \sigma_3^+ + \sigma_2^+ \sigma_3^-) + \frac{g_a^b g_2 g_4}{\delta_2 \delta_4} (\sigma_2^- \sigma_4^+ + \sigma_2^+ \sigma_4^-).
\end{aligned} \tag{A2}$$